



Facile synthesis of $3\text{Li}_2\text{S}-\text{P}_2\text{S}_5:\text{xLiCl}:(1-\text{x})\text{LiI}$ glass ceramic solid electrolyte for solid-state lithium-ion batteries

Rajesh Rajagopal, Kwang-Sun Ryu*

Department of Chemistry, University of Ulsan, Doowang-dong, Nam-gu, Ulsan, 44776, South Korea



ARTICLE INFO

Article history:

Received 6 January 2019

Received in revised form

22 May 2019

Accepted 24 May 2019

Available online 25 May 2019

Keywords:

Solid electrolyte

$3\text{Li}_2\text{S}-\text{P}_2\text{S}_5$

Acetonitrile

LiCl

LiI

Ionic conductivity

ABSTRACT

The $3\text{Li}_2\text{S}-\text{P}_2\text{S}_5:\text{xLiCl}:(1-\text{x})\text{LiI}$ solid electrolytes were prepared via solution process using acetonitrile, and crystallization was achieved by heating at 160°C for 3 h. The crystalline nature and morphology of the prepared materials were studied using powder X-ray diffraction and field emission scanning electron microscope analysis. Cyclic voltammetry was performed to confirm the electrochemical stability of the electrolytes. The ionic conductivity of the prepared $3\text{Li}_2\text{S}-\text{P}_2\text{S}_5:0.25\text{LiCl}:0.75\text{LiI}$ solid electrolyte was $1.32 \times 10^{-4} \text{ S cm}^{-1}$, at room temperature. In addition, the prepared $3\text{Li}_2\text{S}-\text{P}_2\text{S}_5:0.25\text{LiCl}:0.75\text{LiI}$ solid electrolyte showed better electrochemical stability comparable to that of prepared pure $3\text{Li}_2\text{S}-\text{P}_2\text{S}_5$, and other Cl and I mixed solid electrolytes.

© 2019 Elsevier B.V. All rights reserved.

1. Introduction

Recently, the use of solid electrolytes has received great attention because of their numerous advantages and as a substitute for conventional organic liquid electrolytes. To date, various kinds of solid electrolytes, such as inorganic sulfides/oxides and polymers, have been investigated for the development of solid-state Li-ion batteries. The greater advantage of oxide based solid electrolytes is stability in air and ionic conductivity in the order of $10^{-4} \text{ S cm}^{-1}$ with insufficient contact between the electrolyte/electrode interfaces. High-temperature sintering is needed to form lithium ion path due to its large grain boundary. Conversely, sulfide-based solid electrolytes are not stable in air and show lithium ion conductivity in the order of $10^{-3} \text{ S cm}^{-1}$ to $10^{-2} \text{ S cm}^{-1}$ due to the large ionic radii and weaker electro negativity of sulfur ions, which requires low-temperature sintering to form lithium ion path due to its small grain boundary and softness [1,2]. The ionic conductivity of most of the sulfide solid electrolytes is slightly less than that of the conventional organic electrolytes. Even the ionic conductivity of solid electrolytes is less than that of conventional organic electrolytes, and the lithium ion transference number of solid electrolytes (~1) is nearly double that of organic electrolytes (0.5). The high

transference number facilitates fast kinetics and high rate charge-discharge operations [3–5]. In addition, solid sulfide electrolytes exhibit a wide electrochemical window ranging from 5 V to 10 V and negligible electronic conductivity. These characteristics are of great importance for all solid-state batteries in improving the cycle performance. In addition to these sulfide/oxide-based solid electrolytes, researchers have been developing various lithium ionic superconductors (LISCON) such as Li_3YCl_6 , Li_3YBr_6 , Li_3SbS_4 , and LiSe_x to promote high ionic conductivity, and electrochemical and atmospheric stability [6–8].

High interface resistance is a key component of all solid state lithium ion batteries (ASSLIBs), since the high interfacial resistance impedes lithium ion movement between the electrode and electrolyte, and reduces the electrochemical and chemical stability at the interface. Poor contact between the electrolyte and electrode contributes to enhanced interfacial resistance. This poor contact arises from mismatched lattice between two different materials and volume changes during the charging process [9]. Inhomogeneous distribution of solid electrolytes in electrode composite is the reason for poor rate capacity. Recently researcher attempted the fabrication of sheet type ASSLIBs to solve the problem [10,11].

Preparation is another issue for the fabrication of $\text{Li}_2\text{S}-\text{P}_2\text{S}_5$ -based solid electrolytes. $\text{Li}_2\text{S}-\text{P}_2\text{S}_5$ ceramic electrolytes are usually prepared via high-energy ball milling, melt quenching, and solution methods. More recently, liquid phase synthesis has attracted increased attention for the preparation of sulfide solid electrolytes

* Corresponding author.

E-mail address: ryuks@ulsan.ac.kr (K.-S. Ryu).

due to several advantages including reduced time, temperature and scalability during synthesis. These solution-based synthetic approaches generate large-scale product starting from few grams to kilogram compared with planetary ball mill processes providing only gram-scale products. During the synthesis, simply stirring the source material for dissolution in solvent may last few days. In this case, the reaction is promoted by additional processes such as ultrasonication and milling [12–14]. Recently, Dominica et al. prepared pure lithium argyrodite (Li_7PS_6) solid electrolyte in a very short time (2 h) using a pre-synthesized Li_3PS_4 solid electrolyte [15]. In addition, the liquid-phase synthesis resulted in solid electrolytes of small particle size (<500 nm) whereas solid-state synthesis yielded large particles measuring around 10 μm . Interaction between the particles and the solvent and the solvent removal process results in size reduction [16]. Further, the solution-based synthesis offers an easy coating of solid electrolyte layer on active material, which increases the contact area and reduces the interface resistance. Further, these types of coating provide an opportunity to increase the electrode material with high specific capacity [1,16]. Nataly et al. prepared the $\text{Li}_6\text{PS}_5\text{Cl}$ solid electrolyte solution and coated on NCM along with the conductive agent resulting in 80% retention after 20 cycles [17].

Currently, several studies are focusing on the development of

sulfide-based electrolytes with high ionic conductivity, specifically, $\text{Li}_2\text{S}-\text{P}_2\text{S}_5$ binary systems, which strongly depend on the compositional ratio of the base material and the heat-treatment temperature. The ratio between the crystalline and amorphous phases also affects the ionic conductivity of sulfide solid electrolytes [18]. Among various thio-LISCON, Li_3PS_4 attracted great interest due to its high ion conductivity ($>10^{-4} \text{ S cm}^{-1}$), Li compatibility, low temperature synthesis and easy processability. Further, Li_3PS_4 composed of Li^+ and PS_4^{3-} , which is stable in air and releases less H_2S when exposed to air [2]. However most sulfide electrolytes are poor compatibility against lithium metal anodes and oxide-based cathodes is a serious limitation. Specifically, some of the sulfide solid electrolytes, which contain valence variable elements such as Ti, Ge, etc., are not stable when associated with lithium anode. Further sulfide solid electrolytes are oxidized and decomposed into elemental sulfur, sulfides and phosphates by high voltage oxide cathodes upon charge-discharge cycling. Thus, researchers have attempted to improve the electrochemical stability of solid electrolytes by partially substituting the S^{2-} with O^{2-} ions [2,19]. In addition, various metals, halogens, and non-metals can be doped/mixed with a $\text{Li}_2\text{S}-\text{P}_2\text{S}_5$ binary system to improve their ionic conductivities [20], $\text{Li}_{10}\text{GeP}_2\text{S}_{12}$ (LGPS) superionic conductor has been investigated due to its high ionic conductivity (12 mS cm^{-1}).

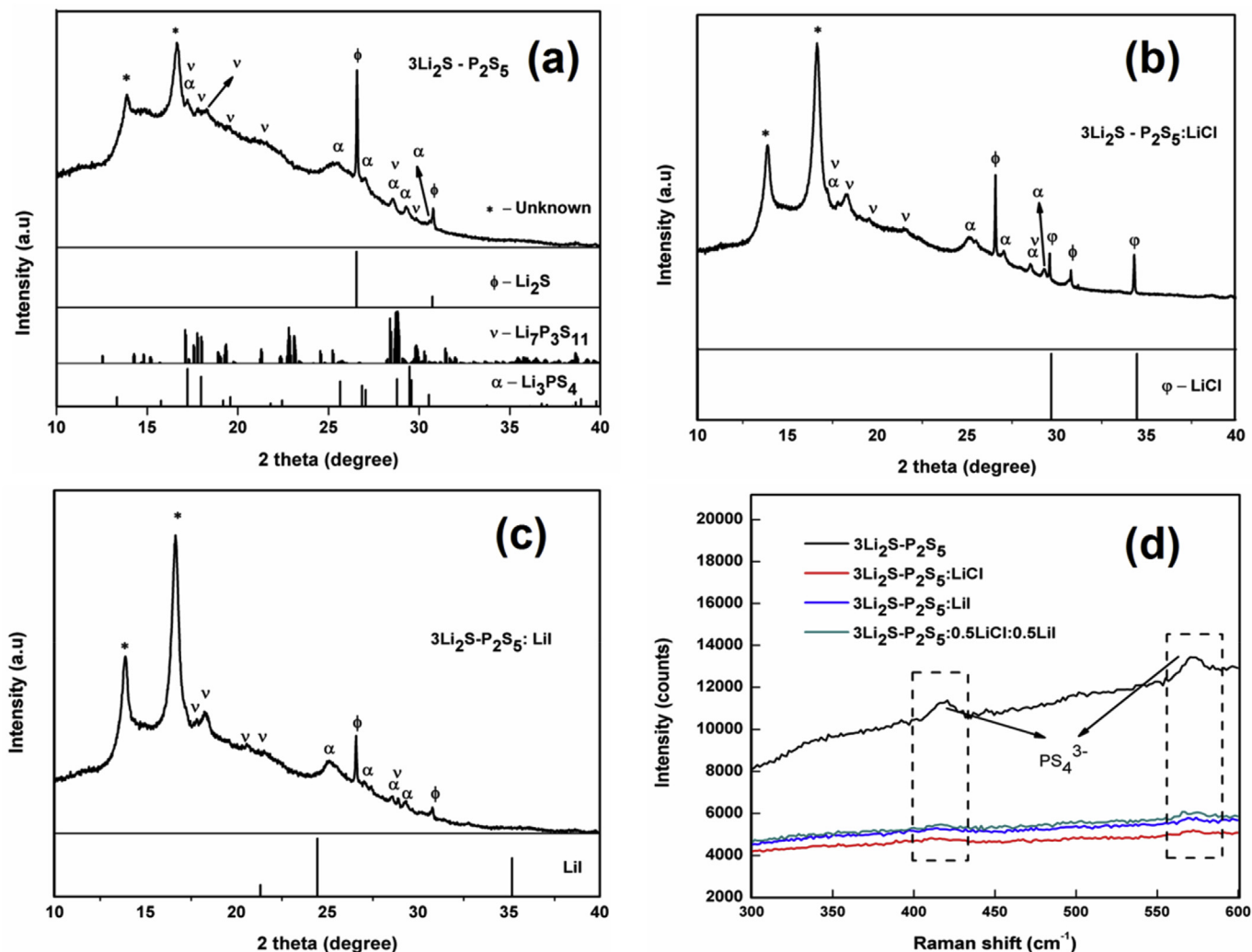


Fig. 1. Powder XRD pattern of (a) $3\text{Li}_2\text{S}\text{-}\text{P}_2\text{S}_5$ and (b) $3\text{Li}_2\text{S}\text{-}\text{P}_2\text{S}_5\text{:LiCl}$ (c) $3\text{Li}_2\text{S}\text{-}\text{P}_2\text{S}_5\text{:LiI}$ glass ceramic pellets and (d) laser Raman spectra of $3\text{Li}_2\text{S}\text{-}\text{P}_2\text{S}_5$, $3\text{Li}_2\text{S}\text{-}\text{P}_2\text{S}_5\text{:LiCl}$, $3\text{Li}_2\text{S}\text{-}\text{P}_2\text{S}_5\text{:LiI}$ and $3\text{Li}_2\text{S}\text{-}\text{P}_2\text{S}_5\text{:0.5LiCl:0.5LiI}$ solid electrolytes.

Unfortunately, LGPS electrolyte shows poor stability due to Ge⁴⁺ ions with a high valance [21]. Thus, it may be appropriate to use inexpensive materials with low valance. Specifically, the addition of lithium halides to Li₂S-P₂S₅ binary system stabilizes the Li-electrolyte interface since the lithium halides are thermodynamically stable against lithium anode [22]. The addition of halogens weakened the interaction between the lithium ions and the surrounding anion framework. This increased site disorder enhances lithium ion vacancy and diffusivity. Further, halogen-doped sulfide solid electrolytes showed a wide electrochemical window up to 10 V [13]. Very few researchers have tried to synthesize Li₂S-P₂S₅ ceramic electrolytes doped with lithium halides by solution synthesis [23–26]. With the above advantages, researchers started using the halogens to thio-NASICONs type electrolytes [27]. Compared with solid electrolytes doped with a single halogen, those doped with two halogens showed high ionic conductivity and low activation energy [9]. Unfortunately, solution-based Li₂S-P₂S₅ ceramic electrolytes doped with bihalides have yet to be reported because using bihalides with Li₂S-P₂S₅ ceramic electrolytes may increase the ionic conductivity. Specifically, iodine and chlorine yield fully ordered S²⁻ and I⁻, and disordered S²⁻ and Cl⁻ structures, respectively. In bihalides, a combination of these ordered and disordered structures may increase lithium ion mobility [19]. On the other hand, LiI has high ionic conductivity than other LiX compounds. Thus, the addition of LiI containing LiCl to the LPS system may increase ionic conductivity.

In this study, we prepared 3Li₂S-P₂S₅ glass ceramic solid electrolyte co-doped with various concentrations of Cl and I via solution synthesis using acetonitrile as the solvent. The prepared glass ceramic electrolyte was characterized by various physiochemical techniques. The electrochemical stability and conductivity of the prepared 3Li₂S-P₂S₅:xLiCl:(1-x)LiI GCS electrolyte was studied by cyclic voltammetry and electrochemical impedance spectroscopy. The electrical conductivity of 3Li₂S-P₂S₅:xLiCl:(1-x)LiI GCS was higher than that of a pure 3Li₂S-P₂S₅GCS electrolyte.

2. Experimental details

2.1. Synthesis and structural characterization of 3Li₂S-P₂S₅ and 3Li₂S-P₂S₅:xLiCl:(1-x)LiI GCS electrolytes

All the experiments were performed in a dry argon atmosphere to avoid exposure to air and moisture. Analytical grade anhydrous Li₂S (99.98%), P₂S₅ (99%), LiCl (99%), LiI (99%), and acetonitrile anhydrous (99.8%) were purchased from Sigma Aldrich and used as received. The 3Li₂S-P₂S₅:LiCl GCS electrolyte was prepared by one-step solution synthesis. Briefly, Li₂S (0.6895 g) P₂S₅ (1.1113 g), and LiCl (0.2115 g) were ground and dissolved in 25 ml of anhydrous acetonitrile (ACN) in a 3:1:1 M ratio and stirred for 24 h. The mixture was not stirred for 5 h to allow the product settle down. The supernatant was carefully removed, and the resultant material was dried at 80 °C for 12 h to obtain a fine powder. Finally, it was heated at 160 °C for 3 h to obtain glass ceramic 3Li₂S-P₂S₅:LiCl solid electrolyte. The above procedure was used to synthesize 3Li₂S-P₂S₅:xLiCl:(1-x)LiI ($x = 0.75, 0.5, 0.25, 0$) GCS electrolytes. Thus the prepared solid electrolytes, 3Li₂S-P₂S₅:LiCl, 3Li₂S-P₂S₅:0.75LiCl:0.25LiI, 3Li₂S-P₂S₅:0.5LiCl:0.5LiI, 3Li₂S-P₂S₅:0.25LiCl:0.75LiI and 3Li₂S-P₂S₅:LiI were designated as LPSCl, LPSCl_{0.75}I_{0.25}, LPSCl_{0.5}I_{0.5}, LPSCl_{0.25}I_{0.75} and LPSI, respectively. For comparison, glass ceramic 3Li₂S-P₂S₅ solid electrolytes were prepared using the same procedure without adding chlorine/iodide and named as LPS.

The crystalline structure of the synthesized 3Li₂S-P₂S₅ and 3Li₂S-P₂S₅:xLiCl:(1-x)LiI GCS electrolytes were analyzed with a high-resolution powder X-ray diffractometer (beamline 9B HRPD at PAL) using a double crystal Si (III) monochromator at a wavelength

of 1.5167 Å with 2θ ranging from 10 to 130.5° (step size = 0.01 s⁻¹). Prior to the XRD analysis, the sample was prepared as a pellet and sealed with a Kapton tape in an argon-filled glove box to prevent damage from oxygen and moisture. Laser Raman spectroscopy was performed to reveal the sulfide structure with an excitation wavelength of 488 nm. The surface morphology and composition of the materials were analyzed using a field-emission scanning electron microscope (FE-SEM, JSM-7610F, Japan) equipped with energy-dispersive X-ray spectroscopy (EDX).

2.2. Coin-cell assembly and electrochemical characterization of 3Li₂S-P₂S₅ and 3Li₂S-P₂S₅:xLiCl:(1-x)LiI electrolytes

The prepared GCS electrolyte (120 mg) was cooled and pressed into a pellet at 300 bar with a radius of 0.7 mm and the thickness of ~0.5 mm. Electrochemical impedance spectroscopy was carried out at frequencies ranging from 5 MHz to 0.01 Hz in an In/SE/In pressure cell. Cyclic voltammetry was performed in the potential window of -0.5–5 V at a scan rate of 1 mV s⁻¹, at room temperature. Before the analysis, a cell with two asymmetrical electrodes with a solid electrolyte pellet was assembled with a stainless steel (SUS) disk as a working electrode and a lithium foil as counter and reference electrodes. Impedance spectroscopy and cycle voltammetry were carried out using the Biologic SP300 instrument.

3. Results and discussion

3.1. Structural characterization of 3Li₂S-P₂S₅, 3Li₂S-P₂S₅:xLiCl:(1-x)LiI glass ceramic solid electrolytes

The powder XRD pattern of prepared and heat-treated 3Li₂S-

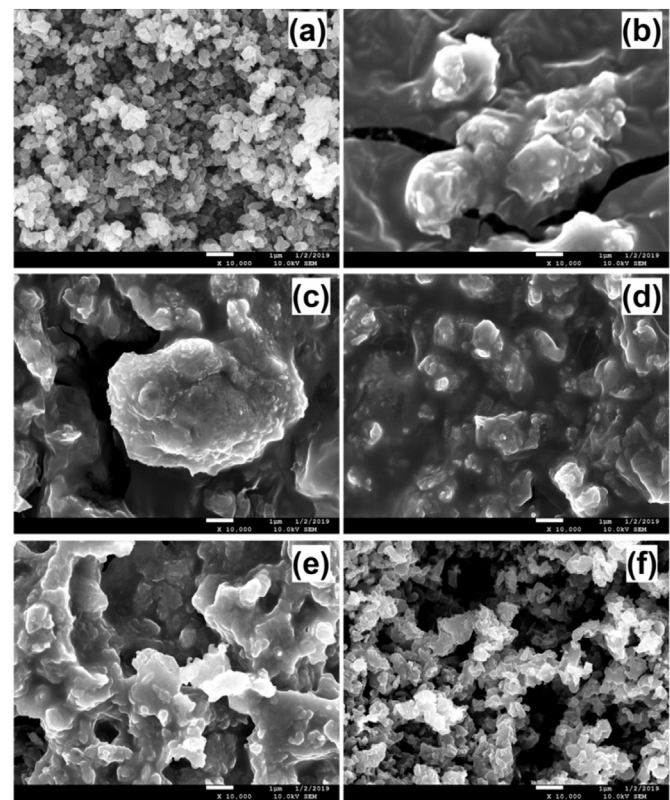


Fig. 2. FE-SEM images of (a) LPS (b) LPSCl, (c) LPSCl_{0.75}I_{0.25}, (d) LPSCl_{0.5}I_{0.5}, (e) LPSCl_{0.25}I_{0.75} and (f) LPSI glass ceramic electrolytes.

P_2S_5 , $3\text{Li}_2\text{S}-\text{P}_2\text{S}_5:\text{LiCl}$ and $3\text{Li}_2\text{S}-\text{P}_2\text{S}_5:\text{LiI}$ glass ceramic pellets are shown in Fig. 1a, b and 1c. The XRD pattern of $3\text{Li}_2\text{S}-\text{P}_2\text{S}_5:\text{LiCl}$ and $3\text{Li}_2\text{S}-\text{P}_2\text{S}_5:\text{LiI}$ was nearly similar to that of $3\text{Li}_2\text{S}-\text{P}_2\text{S}_5$. The XRD analysis of the prepared samples revealed mixed phases, such as $\beta\text{-Li}_3\text{PS}_4$, and $\text{Li}_7\text{P}_3\text{S}_{11}$ [28]. The reference patterns were changed to a wavelength of 1.5167\AA and matched with our XRD results. This mixed phase confirmed the dissolution of the source compounds (Li_2S , P_2S_5 , LiCl , and LiI) and the formation of Li^+ , PS_4^{3-} , S^{2-} , Cl^- and I^- ion species in ACN solution as crystals in different phases during

the heat treatment [29]. The number of $\text{Li}_7\text{P}_3\text{S}_{11}$ peaks (with low intensity) increased in $3\text{Li}_2\text{S}-\text{P}_2\text{S}_5$ electrolyte doped with lithium halides as the lithium halides (LiCl/LiI) interact with $\text{Li}_6\text{P}_2\text{S}_8$ system and produce a $\text{Li}_7\text{P}_3\text{S}_{11}$ ($\text{LiX} + \text{Li}_6\text{P}_2\text{S}_8$) phase. We detected two unknown peaks at $2\theta = 13.8^\circ$ and 16.6° in all samples. Even if these unknown peaks corresponded to pure $\beta\text{-Li}_3\text{PS}_4$ (13.8°) and $\text{Li}_4\text{P}_2\text{S}_6$ (16.6°), the peaks ratios of intensity of the observed and reference patterns differed. The unknown peaks may be attributed to the raw materials and low-temperature heat treatment (160°C) [30–32]. In

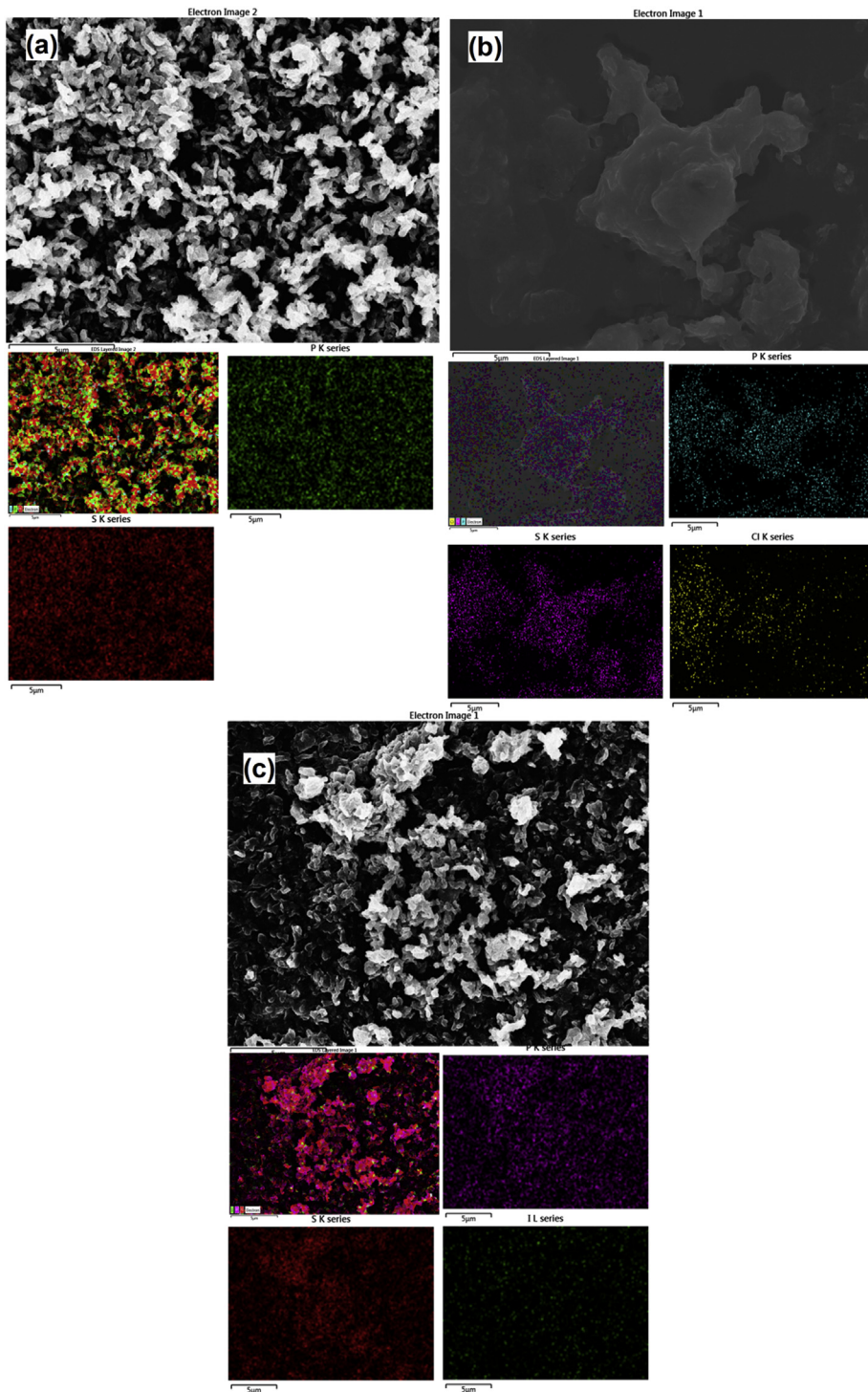


Fig. 3. EDX mapping images of (a) LPS (b) LPSCl and (b) LPSI glass ceramic materials with P, S, Cl and I.

addition, Li_2S residue peaks at 26.6° and 30.7° were detected in all samples. Similarly, LiCl residue peaks at 29.6° and 34.3° were observed in Fig. 1b. Usually, solution-based synthesis yields a small amount of Li_2S residue due to its excessive amounts. During stirring and ultrasonication, Li_2S reacts with P_2S_5 and forms PS_4^{3-} , and first produces LPS composites ($\beta\text{-Li}_3\text{PS}_4$ and $\text{Li}_7\text{P}_3\text{S}_{11}$) which may account for the existence of LPS, Li_2S and LiCl in XRD peaks [29,33,34]. Unfortunately, no LiI or $3\text{Li}_2\text{S}\text{-}\text{P}_2\text{S}_5\text{:LiCl}$ / $3\text{Li}_2\text{S}\text{-}\text{P}_2\text{S}_5\text{:LiI}$ composite peaks were detected suggesting that LiCl and LiI completely dissolved in acetonitrile, and chlorine/iodine may be adsorbed on the surface of LPS crystal lattice. Adsorption of Cl and I ions had no effect on the product phase. However, a small variation was observed in peak position and intensity of $3\text{Li}_2\text{S}\text{-}\text{P}_2\text{S}_5\text{:LiCl}$ and $3\text{Li}_2\text{S}\text{-}\text{P}_2\text{S}_5\text{:LiI}$ composites indicating that proposed synthetic procedure only allowed doping of a small amount of Cl and I ions into the $3\text{Li}_2\text{S}\text{-}\text{P}_2\text{S}_5$ crystal lattice. Since the XRD diffraction of $3\text{Li}_2\text{S}\text{-}\text{P}_2\text{S}_5\text{:LiCl}$ and $3\text{Li}_2\text{S}\text{-}\text{P}_2\text{S}_5\text{:LiI}$ composites are very similar we assumed that the $3\text{Li}_2\text{S}\text{-}\text{P}_2\text{S}_5\text{:xLiCl:(1-x)LiI}$ composites also exhibit similar morphology. No amorphous peaks of the prepared samples were detected, indicating good crystallinity. Fig. 1d shows laser Raman spectra of $3\text{Li}_2\text{S}\text{-}\text{P}_2\text{S}_5$, $3\text{Li}_2\text{S}\text{-}\text{P}_2\text{S}_5\text{:LiCl}$, $3\text{Li}_2\text{S}\text{-}\text{P}_2\text{S}_5\text{:LiI}$ and $3\text{Li}_2\text{S}\text{-}\text{P}_2\text{S}_5\text{:0.5LiCl:0.5LiI}$ solid electrolytes. All samples showed the characteristic peaks around 418 and 570 cm^{-1} confirming the formation of tetrahedral PS_4^{3-} ions. The existence of *ortho*-

thiophosphate (PS_4^{3-}) further confirmed the non-existence of P_2S_5 and reaction with lithium sulfide [35]. The characteristic peaks intensities were reduced after addition of lithium halides. Further, we observed only the PS_4^{3-} characteristic peak indicating the presence of $\beta\text{-Li}_3\text{PS}_4$ and $\text{Li}_7\text{P}_3\text{S}_{11}$ phases. The absence (very small intensity) of $\text{P}_2\text{S}_7^{4-}$ peaks indicates the formation of very low levels of $\text{Li}_7\text{P}_3\text{S}_{11}$ phase. Since $\text{Li}_7\text{P}_3\text{S}_{11}$ phase exhibits PS_4^{3-} and $\text{P}_2\text{S}_7^{4-}$ characteristics peaks [36,37]. The observed laser Raman results adequately matched our XRD results.

Fig. 2 shows the FE-SEM images of $3\text{Li}_2\text{S}\text{-}\text{P}_2\text{S}_5$ and $3\text{Li}_2\text{S}\text{-}\text{P}_2\text{S}_5\text{:xLiCl:(1-x)LiI}$ glass ceramic solid electrolytes. The FE-SEM images of pure $3\text{Li}_2\text{S}\text{-}\text{P}_2\text{S}_5$ GCS electrolyte are illustrated in Fig. 2a. Here we observed nearly spherical particles with an average diameter of $0.5\text{--}0.7\text{ }\mu\text{m}$. The average particle size drastically increased to more than $2\text{ }\mu\text{m}$ with irregular shapes while adding LiCl to $3\text{Li}_2\text{S}\text{-}\text{P}_2\text{S}_5$ ($3\text{Li}_2\text{S}\text{-}\text{P}_2\text{S}_5\text{:LiCl}$) and the corresponding image is shown in Fig. 2b. Gradually increasing LiI (and gradually reducing the corresponding LiCl concentrations) in the above system resulted in decreased particle size and transformed the particles into spherical shape (Fig. 2c–e). The surface morphology of $3\text{Li}_2\text{S}\text{-}\text{P}_2\text{S}_5\text{:LiI}$ was almost similar to that of $3\text{Li}_2\text{S}\text{-}\text{P}_2\text{S}_5$ (Fig. 2f). Thus, we believed that the chlorine ions diffused into LPS system and attracted the nearest particles, resulting in aggregation into larger and irregular particles. Conversely, iodide ions were simply

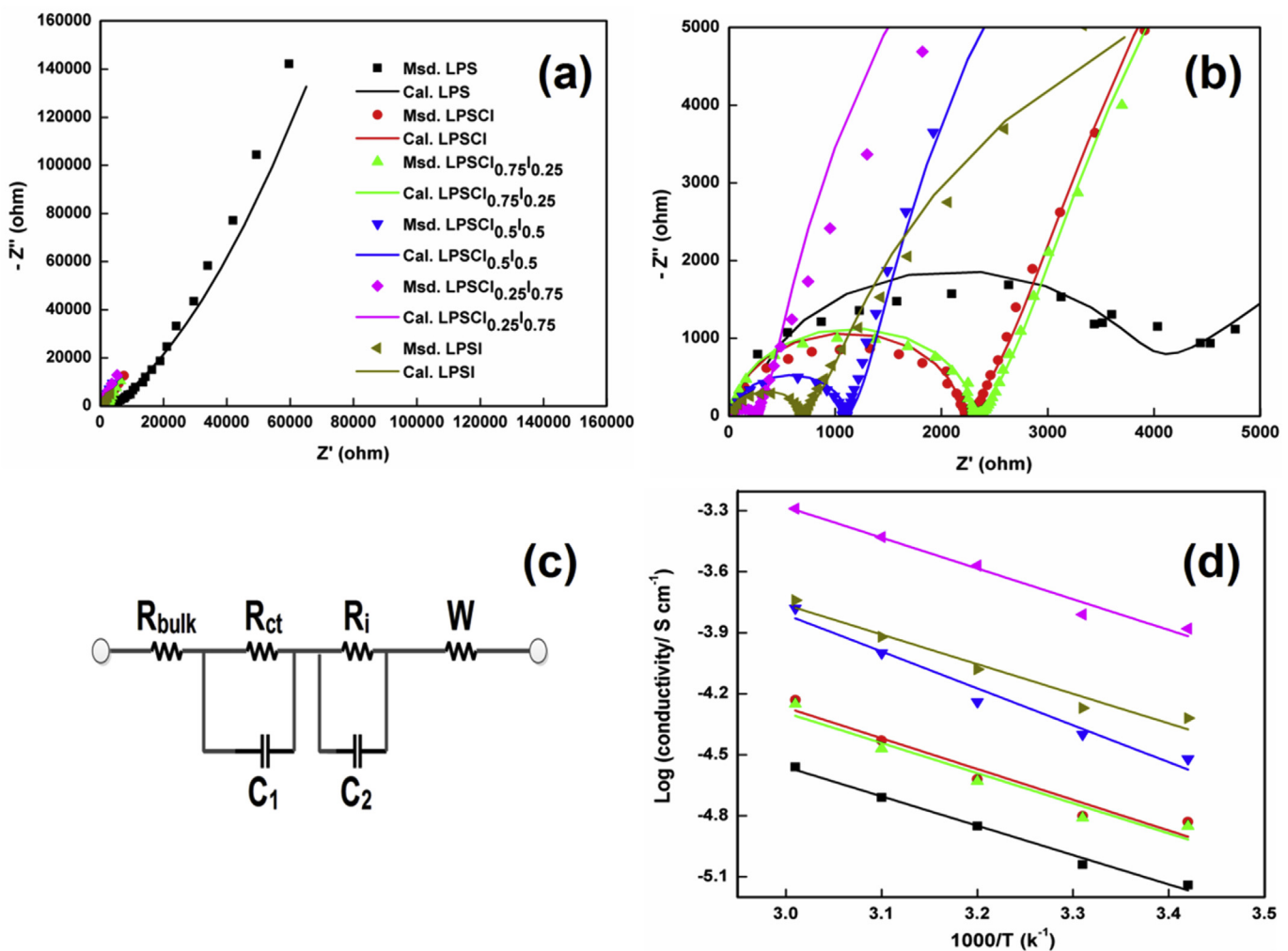


Fig. 4. Nyquist plots of (a and b) $3\text{Li}_2\text{S}\text{-}\text{P}_2\text{S}_5$ and $3\text{Li}_2\text{S}\text{-}\text{P}_2\text{S}_5\text{:xLiCl:(1-x)LiI}$ glass ceramic electrolytes (c) equivalent circuit and (d) Arrhenius plot of $3\text{Li}_2\text{S}\text{-}\text{P}_2\text{S}_5$ and $3\text{Li}_2\text{S}\text{-}\text{P}_2\text{S}_5\text{:xLiCl:(1-x)LiI}$ glass ceramic electrolytes.

attached to the LPS system without aggregation and no or obvious change in particle size or morphology in $3\text{Li}_2\text{S-P}_2\text{S}_5$ or $3\text{Li}_2\text{S-P}_2\text{S}_5:\text{LiI}$.

The energy-dispersive spectroscopy results of $3\text{Li}_2\text{S-P}_2\text{S}_5$, $3\text{Li}_2\text{S-P}_2\text{S}_5:\text{LiI}$

$\text{P}_2\text{S}_5:\text{LiCl}$ and $3\text{Li}_2\text{S-P}_2\text{S}_5:\text{LiI}$ glass ceramic are shown in Fig. 3a, b and c. The EDS mapping analysis revealed uniform distribution of P, S, Cl and I ions.

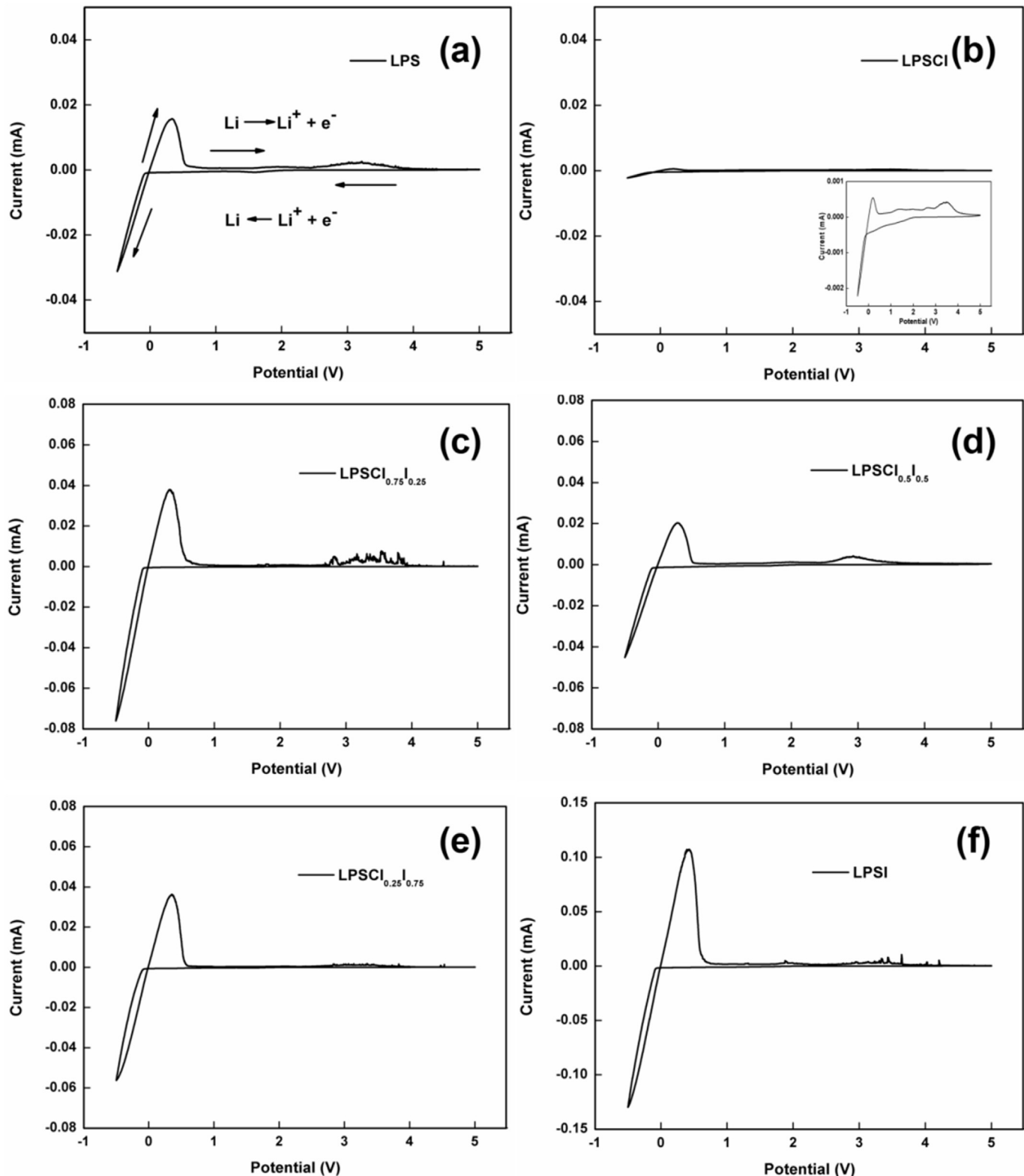


Fig. 5. Cyclic voltammogram plots of (a) LPS (b) LPSCI, (c) $\text{LPSCI}_{0.75}\text{I}_{0.25}$, (d) $\text{LPSCI}_{0.5}\text{I}_{0.5}$, (e) $\text{LPSCI}_{0.25}\text{I}_{0.75}$ and (f) LPSI glass ceramic electrolytes at the scan rate of 1 mV s^{-1} .

3.2. Electrochemical characterization of $3\text{Li}_2\text{S}-\text{P}_2\text{S}_5$ and $3\text{Li}_2\text{S}-\text{P}_2\text{S}_5:\text{xLiCl}:(1-\text{x})\text{LiI}$ GCS electrolytes

The ionic conductivities studies of $3\text{Li}_2\text{S}-\text{P}_2\text{S}_5$ and $3\text{Li}_2\text{S}-\text{P}_2\text{S}_5:\text{xLiCl}:(1-\text{x})\text{LiI}$ GCS electrolytes were analyzed via electrochemical impedance spectroscopy. The measured impedance data were fitted with the Randles circuit using the Zfit tool from Bio-Logic's EC-Lab software and the corresponding measured and fit Nyquist plots are presented in Fig. 4 (a and b). The Nyquist plots of the $3\text{Li}_2\text{S}-\text{P}_2\text{S}_5$ and $3\text{Li}_2\text{S}-\text{P}_2\text{S}_5:\text{xLiCl}:(1-\text{x})\text{LiI}$ samples were adequately fitted with Randles circuit and their corresponding equivalent circuits are presented in Fig. 4c. The total resistance ($R = \text{bulk resistance} (R_{\text{bulk}}) + \text{charge transfer resistance} (R_{\text{ct}}) + \text{interfacial resistance} (R_{\text{i}})$) was used to calculate the ionic conductivity of the prepared solid electrolytes [38]. The calculated ionic conductivity of pure LPS GCS electrolytes was $7.3 \times 10^{-6} \text{ S cm}^{-1}$ at room temperature. Addition of LiCl to pure LPS GCS doubled the total ionic conductivity to $1.78 \times 10^{-5} \text{ S cm}^{-1}$ (LPSCl). Further decreasing the chlorine concentration corresponding to iodine resulted in a gradual increase in the total ionic conductivity. The calculated ionic conductivities of LPSCl_{0.75}I_{0.25} and LPSCl_{0.5}I_{0.5} were 1.43×10^{-5} and $3.0 \times 10^{-5} \text{ S cm}^{-1}$, respectively. LPSCl_{0.25}I_{0.75} glass ceramic solid electrolytes exhibited a high ionic conductivity of $1.32 \times 10^{-4} \text{ S cm}^{-1}$, at room temperature. The ionic conductivity of LPSCl_{0.25}I_{0.75} GCS electrolyte was much higher than that of other lithium halogen doped LPS electrolytes prepared via solution synthesis. We believed that the high ionic conductivity resulted from the combination of large amounts of LiI and $\text{S}^{2-}/\text{Cl}^-$ with high ionic conductivity. LPSCl_{0.75}I_{0.25} and LPSCl_{0.5}I_{0.5} electrolytes contain fewer amounts of LiI and large distribution sites and show better ionic conductivity compared with pure LPS electrolyte alone. Chida et al. synthesized $\text{Li}_6\text{PS}_5\text{Br}$ solid electrolyte via solution method using ethyl propionate-ethanol solution and achieved an ionic conductivity of $3.4 \times 10^{-5} \text{ S cm}^{-1}$, at room temperature [29]. Similarly, Yubuchi et al. prepared $\text{Li}_6\text{PS}_5\text{Cl}$ solid electrolyte using ethanol solution and obtained an ionic conductivity at room temperature of $1.4 \times 10^{-5} \text{ S cm}^{-1}$ without exposure to sintering temperature [39] since the ionic conductivity LiI was higher than that of other lithium halides ($\sigma_{\text{LiI}} > \sigma_{\text{LiBr}} > \sigma_{\text{LiCl}} > \sigma_{\text{LiF}}$) [40]. Unfortunately, the ionic conductivity of LPSI was reduced to $4.8 \times 10^{-5} \text{ S cm}^{-1}$, which may be due to the excessive amount of iodine not permeating inside the LPS system and the absence of $\text{S}^{2-}/\text{Cl}^-$ distribution sites since the ionic conductivity of LiI was in the order of 10^{-6} to $10^{-5} \text{ S cm}^{-1}$ [41]. Usually, solution-processed LPS electrolytes exhibit low ionic conductivity because during the dissolution process all the ions separate and re-crystallize during the sintering process. This process strongly affects the original crystal structure of the LPS electrolytes. Further, the prepared $3\text{Li}_2\text{S}-\text{P}_2\text{S}_5$ and $3\text{Li}_2\text{S}-\text{P}_2\text{S}_5:\text{xLiCl}:(1-\text{x})\text{LiI}$ electrolytes showed less conductivity than other LPS solid electrolytes obtained via high-energy ball milling, perhaps due to large grain boundary resistance [35,42]. These results suggest that our synthesized materials exhibit good conductivity with the glass phase.

Fig. 4d illustrates the temperature dependent ionic conductivity of $3\text{Li}_2\text{S}-\text{P}_2\text{S}_5$ and $3\text{Li}_2\text{S}-\text{P}_2\text{S}_5:\text{xLiCl}:(1-\text{x})\text{LiI}$ GCS electrolytes between 20 and 60 °C. The ionic conductivity of LPS, LPSCl and LPSI GCS electrolytes increased to 2.7×10^{-5} , $6.0 \times 10^{-5} \text{ S cm}^{-1}$ and $1.8 \times 10^{-4} \text{ S cm}^{-1}$, respectively at 60 °C. LPSCl_{0.75}I_{0.25} GCS electrolyte exhibited an ionic conductivity of $5.2 \times 10^{-4} \text{ S cm}^{-1}$ at 60 °C. The temperature-dependent ionic conductivity studies suggested that the LPSCl_{0.75}I_{0.25} GCS electrolyte exhibits better temperature response than $3\text{Li}_2\text{S}-\text{P}_2\text{S}_5$ and other $3\text{Li}_2\text{S}-\text{P}_2\text{S}_5:\text{xLiCl}:(1-\text{x})\text{LiI}$ GCS electrolytes. We have also calculated the activation energy of $3\text{Li}_2\text{S}-\text{P}_2\text{S}_5$ and $3\text{Li}_2\text{S}-\text{P}_2\text{S}_5:\text{xLiCl}:(1-\text{x})\text{LiI}$ GCS electrolytes using Arrhenius equation [28]. The LPSCl_{0.75}I_{0.25} GCS electrolyte showed a low activation energy of $27.23 \text{ kJ mol}^{-1}$. The calculated activation energies of LPS, LPSCl, LPSCl_{0.75}I_{0.25}, LPSCl_{0.5}I_{0.5}, and LPSI, GCS

electrolytes were 27.64, 28.97, 28.06, 34.86, and $29.14 \text{ kJ mol}^{-1}$, respectively. These values matched others obtained via liquid phase synthesis [28,30].

Cyclic voltammetry (CV) has been widely used to analyze the electrochemical stability of inorganic solid electrolytes. The cyclic voltogram plot of a Li/LPS/SUS cell at a scan rate of 1 mV s^{-1} and room temperature is shown in Fig. 5a. Metallic lithium deposition ($\text{Li}^+ + \text{e}^- = \text{Li}$) and slivering ($\text{Li} = \text{Li}^+ + \text{e}^-$) were observed between the potentials of -0.5 – 1 V . In addition, we observed an oxidation peak between 2.5 and 3.5 V compared with the results of ball milling. This oxidation peak may be attributed to the presence of S^{2-} ions [43,44]. The CV plots of doped Li/3Li₂S-P₂S₅:xLiCl:(1-x)LiI/SUS cell are shown in Fig. 5(b–f). Based on the CV graph, we confirmed that the addition of iodine reduced the side reaction between lithium metal and solid electrolyte [45].

4. Conclusions

A sulfide solid electrolyte $3\text{Li}_2\text{S}-\text{P}_2\text{S}_5$ was synthesized using an acetonitrile solvent, and the ionic conductivity was increased by the addition of lithium chloride and lithium iodide. The crystalline nature and morphology of the prepared $3\text{Li}_2\text{S}-\text{P}_2\text{S}_5$ and $3\text{Li}_2\text{S}-\text{P}_2\text{S}_5:\text{xLiCl}:(1-\text{x})\text{LiI}$ glass ceramic electrolytes were studied by XRD and FE-SEM analysis. Compared with $3\text{Li}_2\text{S}-\text{P}_2\text{S}_5$ electrolyte, $3\text{Li}_2\text{S}-\text{P}_2\text{S}_5:\text{0.25LiCl}:\text{0.75LiI}$ glass ceramic electrolyte exhibits a higher ionic conductivity ($1.32 \times 10^{-4} \text{ S cm}^{-1}$ at room temperature) and electrochemical stability. Thus, the presence of chlorine and iodine at a ratio of 1:3 increases the ionic conductivity and is appropriate for the development of solid-state LIBs.

Acknowledgment

This research was supported by the Basic Science Research Program through the National Research Foundation of Korea funded by the Ministry of Education (2018R1D1A3B07050296).

References

- [1] S. Chida, A. Miura, N.C. Rosero-Navarro, M. Higuchi, N.H.H. Phuc, H. Muto, A. Matsuda, K. Tadanaga, Liquid-phase synthesis of $\text{Li}_6\text{PS}_5\text{Br}$ using ultrasonication and application to cathode composite electrodes in all-solid-state batteries, Ceram. Int. 44 (2018) 742–746.
- [2] L. Gaozhan, X. Dongjiao, W. Xuelong, Y. Xiayin, C. Shaojie, X. Ruijuan, L. Hong, X. Xiaoxiong, High air-stability and superior lithium ion conduction of $\text{Li}_{3+}^{3x}\text{P}_{1-x}\text{Zn}_x\text{S}_{4-x}\text{O}_y$ by aliovalent substitution of ZnO for all-solid-state lithium batteries, Energy Storage Mater. 17 (2019) 266–274.
- [3] R.C. Xu, X.H. Xia, S.Z. Zhang, D. Xie, X.L. Wang, J.P. Tu, Interfacial challenges and progress for inorganic all-solid-state lithium batteries, Electrochim. Acta 284 (2018) 177–187.
- [4] L. Qi, G. Zhen, H. Cuiping, F. Yongzhu, L. Song, H. Yan-bing, K. Feiyu, L. Baohua, Challenges and perspectives of garnet solid electrolytes for all solid-state lithium batteries, J. Power Sources 389 (2018) 120–134.
- [5] K. Ömer Ulaş, T. Famprakis, B. Fleutot, B. Marc-David, T. Le Mercier, M. Saiful Islam, C. Masquelier, A review of structural properties and synthesis methods of solid electrolyte materials in the $\text{Li}_2\text{S}-\text{P}_2\text{S}_5$ binary system, J. Power Sources 407 (2018) 31–43.
- [6] W. Shuo, B. Qiang, A.M. Nolan, L. Yunsheng, G. Sheng, S. Qiang, M. Yifei, Lithium chlorides and bromides as promising solid-state chemistries for fast ion conductors with good electrochemical stability, Angew. Chem. Int. Ed. (2019) in press.
- [7] K. Takuya, A. Kato, C. Hotohama, A. Sakuda, A. Hayashi, M. Tatsumisago, Preparation and characterization of lithium ion conductive Li_3SbS_4 glass and glass-ceramic electrolytes, Solid State Ionics 333 (2019) 45–49.
- [8] L. Xiaona, L. Jianwen, L. Jing, W. Changhong, L. Xia, S. Qian, L. Ruying, L. Zhang, Y. Rong, L. Shigang, H. Huan, S. Xueliang, High-Performance $\text{Li}-\text{SeS}_x$ all-solid-state lithium batteries, Adv. Mat. (2019) 1808100.
- [9] W. Heng, Y. Chuang, G. Swapna, E.R.H. van Eck, L. van Eijck, M. Wagenaar, A lithium argyrodite $\text{Li}_6\text{PS}_5\text{Cl}_{0.5}\text{Br}_{0.5}$ electrolyte with improved bulk and interfacial conductivity, J. Power Sources 412 (2019) 29–36.
- [10] Z.D. Hood, W. Hui, A.S. Pandian, R. Peng, K.D. Gilroy, C. Miaofang, L. Chengdu, X. Younan, Fabrication of sub-micrometer-thick solid electrolyte membranes of $\beta\text{-Li}_3\text{PS}_4$ via tiled assembly of nanoscale, plate-like building blocks, Adv. Energy Mat. 8 (2018) 1800014.

- [11] S. Kezheng, A. Shinjo, K. Sakuda, Yamamoto, T. Uchiyama, K. Kuratani, T. Takeuchi, Y. Orikasa, A. Hayashi, M. Tatsumisago, Y. Kimura, T. Nakamura, K. Amezawa, Y. Uchimoto, Morphological effect on reaction distribution influenced by binder materials in composite electrodes for sheet-type all-solid-state lithium-ion batteries with sulfide-based solid electrolyte, *J. Phys. Chem. C* 123 (2019) 3292–3298.
- [12] X. Bai, F. Bo, L. Bin, C. Lu, W. Fang, L. Zhongkuan, Z. Xianghua, M. Hongli, Solvent-assisted ball milling for synthesizing solid electrolyte $\text{Li}_7\text{P}_3\text{S}_{11}$, *J. Am. Ceram. Soc.* 102 (2019) 3402–3410.
- [13] Y. Tokoharu, N.H.H. Phuc, H. Muto, A. Matsuda, Preparation of $\text{Li}_7\text{P}_2\text{S}_8$ solid electrolyte and its application in all-solid-state lithium-ion batteries with graphite anode, *Electron. Mater. Lett.* (2019) 1–6.
- [14] M. Akira, N.C. Rosero-Navarro, A. Sakuda, K. Tadanaga, N.H.H. Phuc, A. Matsuda, N. Machida, A. Hayashi, M. Tatsumisago, Liquid-phase syntheses of sulfide electrolytes for all-solid-state lithium battery, *Nat. Rev. Chem.* (2019) 1.
- [15] D.A. Ziolkowska, W. Arnold, T. Druffel, M. Sunkara, W. Hui, Rapid and Economic Synthesis of a Li_7PS_6 solid electrolyte from a liquid approach, *ACS Appl. Mater. Interfaces* 11 (2019) 6015–6021.
- [16] C. Marcela, N.C. Rosero-Navarro, A. Miura, K. Tadanaga, Electrochemical performance of bulk-type all-solid-state batteries using small-sized $\text{Li}_7\text{P}_3\text{S}_{11}$ solid electrolyte prepared by liquid phase as the ionic conductor in the composite cathode, *Electrochim. Acta* 296 (2019) 473–480.
- [17] N.C. Rosero-Navarro, A. Miura, K. Tadanaga, Preparation of lithium ion conductive $\text{Li}_6\text{PS}_5\text{Cl}$ solid electrolyte from solution for the fabrication of composite cathode of all-solid-state lithium battery, *J. Sol. Gel Sci. Technol.* 89 (2019) 303–309.
- [18] H. Tsukasaki, M. Shigeo, S. Shinya, Y. Hideyuki, Ionic conductivity and crystallization process in the $\text{Li}_2\text{S}-\text{P}_2\text{S}_5$ glass electrolyte, *Solid State Ionics* 317 (2018) 122–126.
- [19] Z. Zhixia, Z. Long, Y. Xinlin, W. Hongqiang, L. Yanyan, Y. Chuang, C. Xiaoting, L. van Eijck, W. Bin, All-in-one improvement toward $\text{Li}_6\text{PS}_5\text{Br}$ -based solid electrolytes triggered by compositional tune, *J. Power Sources* 410 (2019) 162–170.
- [20] Z. Feng, M. Kotobuki, S. Shufeng, L. Man On, L. Lu, Review on solid electrolytes for all-solid-state lithium-ion batteries, *J. Power Sources* 389 (2018) 198–213.
- [21] X. Dongjiu, C. Shaojie, Z. Zhihua, R. Jie, Y. Lili, W. Linbin, Y. Xiayin, X. Xiaoxiong, High ion conductive Sb_2O_5 -doped β - Li_3PS_4 with excellent stability against Li for all-solid-state lithium batteries, *J. Power Sources* 389 (2018) 140–147.
- [22] M. Suyama, A. Kato, A. Sakuda, A. Hayashi, M. Tatsumisago, Lithium dissolution/deposition behavior with $\text{Li}_3\text{PS}_4\text{-LiI}$ electrolyte for all-solid-state batteries operating at high temperatures, *Electrochim. Acta* 286 (2018) 158–162.
- [23] N.C. Rosero-Navarro, T. Kinoshita, A. Miura, M. Higuchi, K. Tadanaga, Effect of the binder content on the electrochemical performance of composite cathode using $\text{Li}_6\text{PS}_5\text{Cl}$ precursor solution in an all-solid-state lithium battery, *Ionics* 23 (2017) 1619–1624.
- [24] S. Xiaolin, S. Yimin, C. Fengting, L. Xichao, S. Shimei, L. Tao, W. Jianfei, Preparation, characterization and ionic conductivity studies of composite sulfide solid electrolyte, *J. Alloy. Comp.* 727 (2017) 1136–1141.
- [25] S.J. Sedlmaier, S. Indris, C. Dietrich, M. Yavuz, C. Dräger, F. von Seggern, H. Sommer, J. Janek, $\text{Li}_4\text{PS}_4\text{I}$: A Li^+ superionic conductor synthesized by a solvent-based soft chemistry approach, *Chem. Mater.* 29 (2017) 1830–1835.
- [26] Z. Jun, Z. Chao, L. Jiatao, X. Yang, L. Chu, H. Hui, G. Yongping, T. Xinyong, Z. Wenku, Poly (ethylene oxide) reinforced $\text{Li}_6\text{PS}_5\text{Cl}$ composite solid electrolyte for all-solid-state lithium battery: Enhanced electrochemical performance, mechanical property and interfacial stability, *J. Power Sources* 412 (2019) 78–85.
- [27] U. Miwa, S. Yubuchi, F. Tsuji, A. Sakuda, A. Hayashi, M. Tatsumisago, Suspension synthesis of $\text{Na}_{3-x}\text{PS}_{4-x}\text{Cl}_x$ solid electrolytes, *J. Power Sources* 428 (2019) 131–135.
- [28] W. Yuxing, L. Dongping, B. Mark, P.Z. El Khoury, H. Kee Sung, D. Zhiqun Daniel, X. Jie, Z. Ji-Guang, L. Jun, Mechanism of formation of $\text{Li}_7\text{P}_3\text{S}_{11}$ solid electrolytes through liquid phase synthesis, *Chem. Mater.* 30 (2018) 990–997.
- [29] C. Shunjiro, A. Miura, N.C. Rosero-Navarro, M. Higuchi, N.H.H. Phuc, H. Muto, A. Matsuda, K. Tadanaga, Liquid-phase synthesis of $\text{Li}_6\text{PS}_5\text{Br}$ using ultrasonication and application to cathode composite electrodes in all-solid-state batteries, *Ceram. Int.* 44 (2018) 742–746.
- [30] P. Nguyen Huu Huy, M. Totani, K. Morikawa, H. Muto, A. Matsuda, Preparation of Li_3PS_4 solid electrolyte using ethyl acetate as synthetic medium, *Solid State Ionics* 288 (2016) 240–243.
- [31] C. Sunho, A. Jiu Ann, D. Jiyae, L. Seungwoo, P. Chanhwi, S. Dongwook, Application of rod-like $\text{Li}_6\text{PS}_5\text{Cl}$ directly synthesized by a liquid phase process to sheet-type electrodes for all-solid-state lithium batteries, *J. Electrochem. Soc.* 166 (2019) A5193–A5200.
- [32] L. Zengcai, F. Wujun, E. Andrew Payzant, Y. Xiang, W. Zili, N.J. Dudney, J. Kiggans, K. Hong, A.J. Rondinone, L. Chengdu, Anomalous high ionic conductivity of nanoporous β - Li_3PS_4 , *J. Am. Chem. Soc.* 135 (2013) 975–978.
- [33] C. Marcela, N.C. Rosero-Navarro, A. Miura, K. Tadanaga, Instantaneous preparation of high lithium-ion conducting sulfide solid electrolyte $\text{Li}_7\text{P}_3\text{S}_{11}$ by a liquid phase process, *RSC Adv.* 7 (2017) 46499–46504.
- [34] C. Seon-Joo, L. Sang-Hun, H. Yoon-Cheol, Y. Ji-Hyun, D. Chil-Hoon, L. Youjin, P. Jun-Woo, L. Sang-Min, S. Heon-Cheol, Synthesis and electrochemical characterization of a glass-ceramic $\text{Li}_7\text{P}_2\text{S}_8$ solid electrolyte for all-solid-state Li-ion batteries, *J. Electrochem. Soc.* 165 (2018) A957–A962.
- [35] D. Liu, W. Zhu, Z. Feng, A. Guerfi, A. Vijn, K. Zaghib, Recent progress in sulfide-based solid electrolytes for Li-ion batteries, *Mater. Sci. Eng., B* 213 (2016) 169–176.
- [36] C. Shaojie, X. Dongjiu, L. Gaozhan, J.P. Mwizerwa, Z. Qiang, Z. Yanran, X. Xiaoxiong, Y. Xiayin, Sulfide solid electrolytes for all-solid-state lithium batteries: Structure, conductivity, stability and application, *Energy Storage Mater.* 14 (2018) 58–74.
- [37] A. Yasuhito, O. Kengo, N. Takeshi, H. Yuichi, S. Yoko, K. Toshikatsu, T. Mitsuhashi, Chemical and structural changes of $70\text{Li}_2\text{S}-30\text{P}_2\text{S}_5$ solid electrolyte during heat treatment, *Solid State Ionics* 310 (2017) 50–55.
- [38] R.C. Xu, X.H. Xia, Z.J. Yao, X.L. Wang, C.D. Gu, J.P. Tu, Preparation of $\text{Li}_7\text{P}_3\text{S}_{11}$ glass-ceramic electrolyte by dissolution-evaporation method for all-solid-state lithium ion batteries, *Electrochim. Acta* 219 (2016) 235–240.
- [39] S. Yubuchi, T. Shingo, A. Keigo, T. Kiyoharu, H. Akitoshi, T. Masahiro, Preparation of high lithium-ion conducting $\text{Li}_6\text{PS}_5\text{Cl}$ solid electrolyte from ethanol solution for all-solid-state lithium batteries, *J. Power Sources* 293 (2015) 941–945.
- [40] M. Rene, M. Jean-Pierre, F. Bernard, R. Guy, Superionic conduction in $\text{Li}_2\text{S}-\text{P}_2\text{S}_5\text{-LiI}$ -glasses, *Solid State Ionics* 5 (1981) 663–666.
- [41] C.C. Liang, Conduction characteristics of the lithium iodide-aluminum oxide solid electrolytes, *J. Electrochem. Soc.* 120 (1973) 1289–1292.
- [42] R. Ezhiyilmurugan, L. Zengcai, G. Mallory, P. Kartik, S. Gayatri, Z. Wei, W. Hui, G. Steve, L. Chengdu, An iodide-based $\text{Li}_7\text{P}_2\text{S}_8$ superionic conductor, *J. Am. Chem. Soc.* 137 (2015) 1384–1387.
- [43] U. Satoshi, H. Akitoshi, T. Masahiro, Structure, ionic conductivity and electrochemical stability of $\text{Li}_2\text{S}-\text{P}_2\text{S}_5\text{-LiI}$ glass and glass–ceramic electrolytes, *Solid State Ionics* 211 (2012) 42–45.
- [44] B. Sylvain, C. Matthieu, T. Jean-Marie, V. Virginie, Mechanochemical synthesis of Li-argyrodite $\text{Li}_6\text{PS}_5\text{X}$ ($\text{X} = \text{Cl}, \text{Br}, \text{I}$) as sulfur-based solid electrolytes for all solid state batteries application, *Solid State Ionics* 221 (2012) 1–5.
- [45] X. Ruo-chen, X. Xin-hui, W. Xiu-li, X. Yan, T. Jiang-ping, Tailored $\text{Li}_2\text{S}-\text{P}_2\text{S}_5$ glass-ceramic electrolyte by MoS_2 doping, possessing high ionic conductivity for all-solid-state lithium-sulfur batteries, *J. Mater. Chem. C* 5 (2017) 2829–2834.